Turkish Journal of Physics

http://journals.tubitak.gov.tr/physics/

Research Article

Turk J Phys
(2017) 41: 124 – 132

doi:10.3906/fiz-1610-6

Comparison of structural properties of some liquid crystals

E. Mine ÇAPAR*
Department of Physics, Faculty of Science, Ege University, İzmir, Turkey

Received: 04.10.2016 • **Accepted/Published Online:** 27.12.2016 • **Final Version:** 18.04.2017

Abstract: Molecular dynamics simulations were performed for three liquid crystalline molecules, 4-cyano-4′-octyloxybiphenyl (8OCB), n-p-cyanobenzylidene-p-octyloxyaniline (CBOOA), and p-n-hexyloxybenzylidene-p′-aminobenzonitrile (HBAB). Simulation data were obtained for three liquid crystals in the nematic and isotropic phases to analyze their structural properties. The imine spacer group in the Schiff bases induces a stepped core structure in which the linearity is maintained. The distributions of the angles between some defined vectors imply that the core segments of CBOOA and HBAB are more floppy than the 8OCB core. The biaxialities, molecular dimensions, and molecular anisotropies were calculated. The results were compared for three mesogens in the nematic and isotropic phases.

Key words: Liquid crystals, Schiff base, molecular dynamics simulation, structural properties

1. Introduction

Liquid crystals (LCs) have been employed in a range of important electrooptic devices including today's mobile phones, laptops, and flat panel televisions [1–3]. Many biological materials give structural features that are closely related to those of liquid crystals [4]. Therefore, mesophases have attracted special scientific attention that can be ascribed to a need for understanding of biological systems and to many technical applications.

A combination of theoretical aspects of statistical mechanics, computer simulations, and experiments provides a useful approach to establish a relationship between liquid-crystalline properties and molecular structure [5–8]. Over the last decade, with the increase of computational power, molecular dynamics (MD) simulations have been used to study mesophases in more detail. Recently, a number of MD simulation studies of LCs have been carried out with not only less complex molecular models [9] but also to obtain additional information on a molecular level with very complex atomistic models [10]. Atomistic simulations can yield a wealth of information about liquid crystal phases. These include elastic constants [11,12], order parameters [13], flexoelectric coefficients [14,15], transport properties [16–18], and static and frequency-dependent dielectric constants [19,20]. Recent lengthy atomistic MD simulations performed to reproduce nematic to isotropic transition temperatures have given satisfactory results for two homolog series, namely phenyl alkyl-4-(4′-cyanobenzelidene) aminocynnamates [21] and 4-n-alkyl-4′-cyanobiphenyls [22-24]. Furthermore, these MD simulations have successfully predicted the odd-even effect observed by Gray and Harrison [25]. These encouraging results motivated us to investigate structural properties of cyano compounds different from the previously investigated ones by means of atomistic MD simulations.

There has been considerable interest in the strongly polar cyanobiphenyl-based liquid crystals with the

*Correspondence: mine.capar@ege.edu.tr

observation of the twisted nematic effect by Schadt and Helfrich [26]. Schiff bases and alkoxy biphenyls with cyano substituents along their long molecular axis are commonly employed in twisted nematic displays with low threshold voltages. To widen the nematic range, their eutectic mixtures are used [27,28]. The other reason why many reports are still concerned with these types of materials is reentrant behavior in these LCs discovered by Cladis [29]. The reentrant nematic phase of 4-cyano-4′-octyloxybiphenyl (8OCB) was observed at high pressure [30]. In certain binary mixtures of 8OCB, n-p-cyanobenzylidene-p-octyloxyaniline (CBOOA) and p-n-hexyloxybenzylidene-p′-aminobenzonitrile (HBAB) exhibit the reentrant nematic phase [31].

The cyanobiphenyl and two Schiff bases with alkoxy end groups chosen in this work were three typical liquid crystals, 8OCB, CBOOA, and HBAB. In this study, atomistic MD simulations for 8OCB, CBOOA, and HBAB in the nematic and isotropic phases were performed. In the following, the results of simulations on 8OCB, CBOOA, and HBAB are reported and their structural properties are compared.

2. Materials and methods

2.1. Molecular dynamics simulation

Atomistic MD calculations on three samples each consisting of 8OCB, CBOOA, or HBAB molecules were carried out by using GROMACS (version 4.5.5) software [32]. In each system modeled as in Figure 1, the aromatic hydrogens were explicitly considered, while the CH_2 and CH_3 groups were treated as single interaction centers.

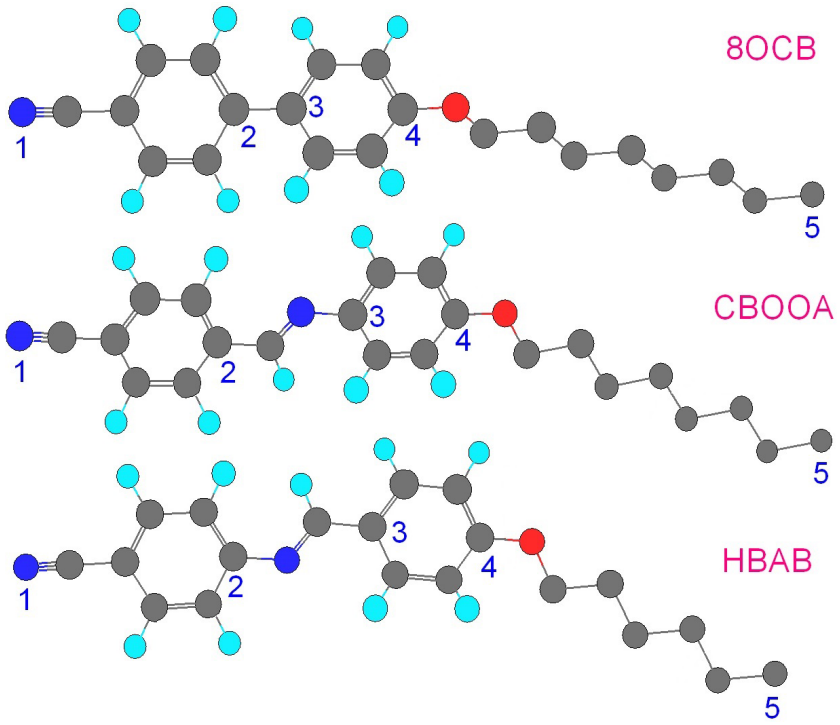

Figure 1. Assignment of the molecular models for the three molecules with the numbering of five atoms: (a) 4-cyano-4′-octyloxybiphenyl (8OCB), (b) n-p-cyanobenzylidene-p-octyloxyaniline (CBOOA), (c) p-n-hexyloxybenzylidene-p′-aminobenzonitrile (HBAB).

The bonding and nonbonding interactions of mesogens were based on the OPLS force field [33,34] using some additional parameters taken from previous studies [21,35]. The fractional atomic charges were determined

by using the CHELPG [36] scheme following the Hartree–Fock geometry optimization with a 6-31G** basis set. The charges were calculated with the GAUSSIAN 03 program package [37]. Bond stretching was explicitly considered and a time step of 0.5 fs was used for the integration. Nonbonding interactions were truncated by a cutoff radius of 1 nm. Periodic boundary conditions were applied in all three dimensions. The long-range electrostatic interactions were evaluated with the particle-mesh Ewald method [38].

Initially, each simulation was started from a cubic lattice of 512 molecules oriented with perfect order at a low density. The orientations of the molecules were altered in order to prevent a net dipole moment from occurring. The systems at low density were compressed by high pressure ($P = 50$ atm) at the initial temperature of 250 K. The configurations for which the system density almost equaled 1 g/cm^3 were chosen as initial configurations for equilibration, and then each system was equilibrated at atmospheric pressure by slowly increasing the initial temperature to 346 K, 373 K, and 368 K for nematic 8OCB, CBOOA, and HBAB, respectively, while the temperatures were increased to 500 K for isotropic 8OCB and to 530 K for isotropic CBOOA and HBAB. In the NPT ensemble, a v-rescale thermostat [39] and Berendsen barostat [40] were used.

The molecular long axis was found by the diagonalization of the inertial tensor:

$$I_{ab} = \sum_{i=1}^{N} m_i \left(r_i^2 \delta_{ab} - r_{ia} r_{ib} \right), \tag{1}$$

where r_i and m_i are the positions relative to the molecular center of mass and the masses of the atoms, respectively. The diagonal tensor components are averaged over all the molecules and all the configurations for a given MD trajectory. The molecular axis unit vector u is the eigenvector corresponding to the smallest eigenvalue of I_{ab} .

The instantaneous nematic director was determined from the second-rank alignment tensor Q_{ab}:

$$Q_{ab} = \frac{1}{N} \sum_{i=1}^{N} \left(\frac{3u_{ia}u_{ib} - \delta_{ab}}{2} \right) \quad \{a, b = x, y, z\}, \tag{2}$$

where N is the number of simulated molecules, and u_{ia} and u_{ib} are the Cartesian components of a unit vector $\mathbf{u}_i$ along the molecular long axis. The time and ensemble average of the largest eigenvalue of the ordering matrix Q_{ab} is equal to the orientational order parameter S_2 and the associated eigenvector gives the director $\mathbf{n}$.

It is important to determine the molecular aspect ratio, anisotropy ΔT, and biaxiality λ_T of certain conformation-dependent molecular properties T because of their effects on LC phase behavior. In this study, the shape and inertia tensor anisotropies, ΔL and ΔI, and the biaxialities obtained from molecular dimensions and inertia tensor components, λ_L and λ_I, were calculated by using Eqs. (3) and (4), respectively, as suggested in previous studies [21, 24].

$$\Delta T = \frac{T_{zz} - (T_{xx} + T_{yy})/2}{T_{xx} + T_{yy} + T_{zz}} \tag{3}$$

$$\lambda_T = \sqrt{\frac{3}{2}} \left(\frac{T_{xx} - T_{yy}}{2T_{zz} - T_{xx-}T_{yy}} \right) \tag{4}$$

3. Results

In order to monitor the equilibration of the systems, the time evolution of the order parameter S_2 was as given in Figure 2. As seen from the figure, the order parameter for each mesogen stays in a steady state for long times in the nematic phase although it fluctuates in the isotropic phase, and for each run the last 10 ns of the trajectories was used for analysis.

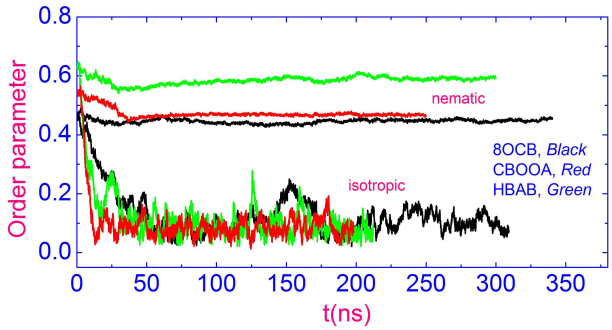

Figure 2. The order parameter S_2 as a function of the simulation time for 8OCB, CBOOA, and HBAB in the nematic and isotropic phases.

The average second rank order parameters of 8OCB, CBOOA, and HBAB samples in the nematic phase were calculated in this study to be 0.45, 0.47, and 0.59, respectively. The corresponding experimental nematic order parameters of 0.44 [41], 0.42 [42], and 0.48 [43] agree satisfactorily with the MD results. The order parameters were found as 0.08 for 8OCB and CBOOA and as 0.07 for HBAB in the isotropic phase and these calculated values are in the range accepted for isotropics [21].

To discuss the orientational behaviors of the three mesogens, the distribution of some angles between interatomic vectors $\vec{V}_{ij}$ from atom i to j (i, j = 1,..,5 as described in Figure 1) have been used. The angle α is between $\vec{V}_{12}$ and $\vec{V}_{23}$, with β the angle between $\vec{V}_{12}$ and $\vec{V}_{35}$ vectors and γ the angle between $\vec{V}_{12}$ and $\vec{V}_{34}$. In Figure 3, the distributions of the angles α, β, and γ obtained from the simulations are shown. In the nematic and isotropic phases, the distributions for angle α show a relatively narrow peak at $\sim 5^\circ$ for 8OCB and two broader almost coincident peaks at $\sim 18^\circ$ for CBOOA and HBAB (Figure 3a). $\vec{V}_{12}$ is nearly in the same direction as $\vec{V}_{23}$ for 8OCB, whereas imine (-CH=N-) linking groups give rise to an increase in the most probable α. The marked difference between the peak widths seen in Figure 3a means that the core segments of the two Schiff bases are more floppy than the core of 8OCB having no linkage group. The distributions of β in Figure 3b are substantially broader than the corresponding α distributions due to flexibility in alkoxy chains. Since the alkoxy chain lengths of 8OCB and CBOOA are the same, their peaks quite coincide. The β distribution for HBAB in the nematic phase, which has the shortest alkoxy chain, exhibits a slightly sharper peak in the histogram graph than those of other compounds. Figure 3c shows that the distributions of γ are sharper than those of β as a result of the rigidity of each phenyl ring. The peaks for the two Schiff bases ($\sim 10^\circ$) are this time close to the 8OCB peak at $\sim 5^\circ$ for both phases. It can be concluded from Figure 3c that the imine spacer group gives rise to a core structure having step, but the linearity is kept. As seen in Figure 3, in the isotropic phase the peak positions of the distributions of α, β, and γ for three mesogens shift slightly to greater values, and the distributions are somewhat broader because of the increment in the flexibility of the mesogens.

Figures 4a and 4b illustrate probability distribution functions of the angle between the molecular axis unit vector **u** and $\vec{V}_{14}$ and $\vec{V}_{45}$, respectively. In Figure 4 there are two maxima for each mesogen because

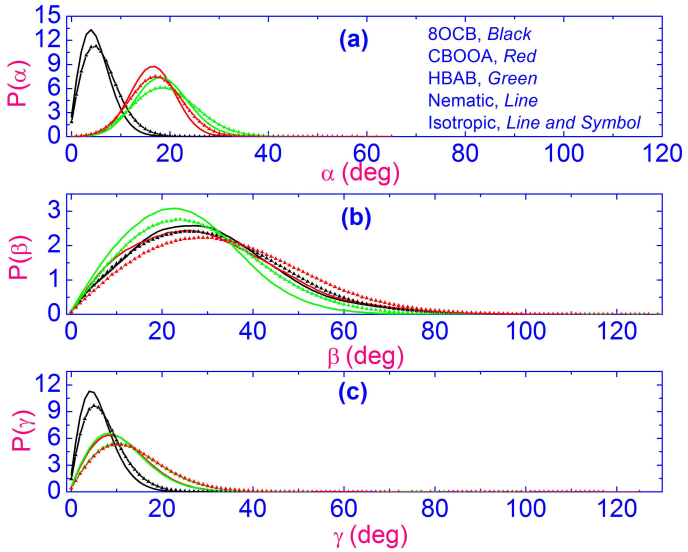

Figure 3. Probability distribution functions (a) $P(\alpha)$, (b) $P(\beta)$, and (c) $P(\gamma)$ for 8OCB, CBOOA, and HBAB.

of the direction of **u** and –**u** of the molecules and the positions of the two maxima are symmetric relative to the middle point of the x-axis in the figure, which corresponds to 90°. In Figure 4a, the positions of the maxima of 8OCB are at ∼18° and ∼160°. The positions of the left and right maxima of the CBOOA and HBAB compounds having imine linking groups sequentially move through 0° and 180°, respectively and their distributions are narrower and sharper than the peaks of 8OCB. The positions of the maxima of HBAB are at ∼10° and ∼170°. Therefore, $\vec{V}_{14}$ is oriented in almost the same direction as **u** and –**u** for HBAB, i.e. the rigid part is along the molecular axis, probably due to the short alkoxy chain, being different from CBOOA. The curve in Figure 4b represents the distribution of the angle between $\vec{V}_{45}$ and the long axis of each molecule, showing the same tendency for each mesogen. The peaks get slightly broader in Figure 4b because of the flexibility of the alkyl chain. It is found that all distributions in Figure 4 slightly expand in the isotropic phase. To make the illustration clear, the distribution function of the angle between the molecular axes of unit vector **u** and $\vec{V}_{14}$ for CBOOA molecules in the isotropic phase is given as an example in Figure 4a.

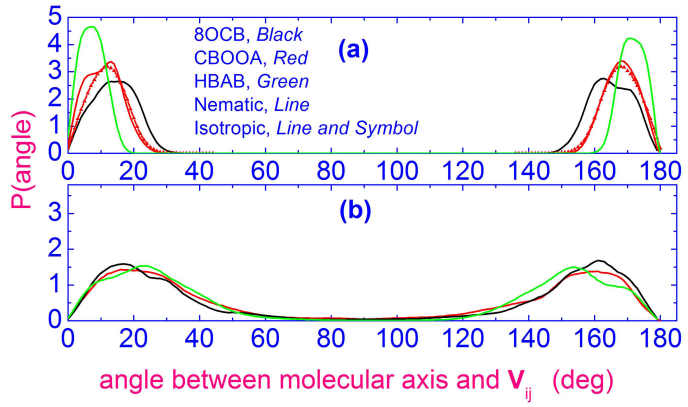

Figure 4. Distribution functions of the angle between molecular axis **u** and (a) $\vec{V}_{14}$ and (b) $\vec{V}_{45}$ for 8OCB, CBOOA, and HBAB.

The molecular length L_z is computed by projecting the position vector between two end atoms along the long molecular axis, which corresponds to the smallest eigenvalue of the inertia matrix, and then adding the Lennard–Jones atomic radii of the related atoms to the projection. The molecular width is determined as the diameter of the minimum cylinder containing the entire molecule. In Table 1, the average molecular length and width $\langle w\rangle = (\langle L_x\rangle + \langle L_y\rangle)/2$, the aspect ratio $\langle L_z\rangle/\langle w\rangle$ together with the anisotropy ΔL, and the biaxiality λ_L of the molecular length are presented. If we compare the molecular dimensions of 8OCB and CBOOA, which have the same alkoxy chain lengths, it can be understood that the imine group of CBOOA increases the molecular dimensions considerably with respect to 8OCB. The average molecular length of HBAB molecule with the imine group and with the shortest alkyl chain has a value between the molecular lengths of the other two mesogens, and it has the smallest width. The molecules with an imine group have greater aspect ratio and shape anisotropy than these values of 8OCB. The calculated molecular lengths are in agreement with the experimental results [44]. As seen from Table 1, $\langle L_x\rangle$ and $\langle L_y\rangle$ are unequal and the shape biaxialities for nematic 8OCB, CBOOA, and HBAB are calculated to be 0.122, 0.102, and 0.075, respectively, being in the order of the biaxiality parameters measured by Madsen et al. [45]. The biaxialities for Schiff bases are higher than the ones computed for the series of aminocinnamates [21] but they are smaller than the biaxiality of 8OCB in this study. In the isotropic phase, the flexibility of the mesogens especially increases the conformational mobility supplied by the flexible alkoxy chain. Therefore, as is understood from Table 1, the molecular length, aspect ratio, and shape anisotropy decrease and the molecular width and biaxiality increase.

Table 1. Average molecular dimensions (Å), aspect ratio $\langle L_z\rangle/\langle w\rangle$, anisotropy $\langle \Delta L\rangle$, and biaxiality $\langle \lambda_L\rangle$ for 8OCB, CBOOA, and HBAB in the nematic and isotropic phases. The experimental values in parentheses were predicted by Cladis [44]. *: Isotropic phase.

Molecules	$\langle L_x\rangle$	$\langle L_y\rangle$	$\langle L_z\rangle$	$\langle \Delta L\rangle$	$\langle \lambda_L\rangle$	$\langle w\rangle$	$\frac{\langle L_z\rangle}{\langle w\rangle}$
8OCB	8.39	5.87	20.87 (23.1)	0.391	0.122	7.13	2.98
8OCB*	8.49	5.93	20.61	0.382	0.128	7.21	2.92
CBOOA	8.55	6.17	22.84 (26.4)	0.412	0.102	7.36	3.10
CBOOA*	8.80	6.28	22.39	0.396	0.114	7.54	3.02
HBAB	7.77	6.04	21.50 (24.2)	0.414	0.075	6.90	3.11
HBAB*	7.92	6.11	21.24	0.404	0.081	7.01	3.03

Table 2. Average principal inertia tensor components (amu Å^2), anisotropy $\langle \Delta \mathbf{L}\rangle$, and biaxiality $\langle \lambda_I\rangle$ for 8OCB, CBOOA, and HBAB in the nematic and isotropic phases. *: Isotropic phase.

Molecules	$\langle I_{xx}\rangle$	$\langle I_{yy}\rangle$	$\langle I_{zz}\rangle$	$\langle \Delta \mathbf{L}\rangle$	$\langle \lambda_I\rangle$
8OCB	8377	8782	647	–0.442	0.035
8OCB*	8221	8642	675	–0.439	0.038
CBOOA	11,406	11,845	731	–0.452	0.028
CBOOA*	11,054	11,551	807	–0.446	0.033
HBAB	9005	9251	500	–0.459	0.018
HBAB*	8869	9134	528	–0.456	0.020

The distribution functions of the molecular lengths in Figure 5a are very broad, thus implying that there are many molecules not being in all-trans conformation. The presence of the imine group as a spacer in CBOOA leads to a considerable increment in the most probable molecular length and a shift in the entire distribution

curve towards longer distance when it is compared with the distribution for 8OCB. In Figure 5b, the molecular width distributions of Schiff bases give a double peak. The right shoulder for the CBOOA molecule moves to higher values. For HBAB molecules with short alkyl chains, the molecular length and breadth distributions are narrower than these of both CBOOA and 8OCB. It may be thought that the HBAB molecule has restricted conformational mobility, and so HBAB has a higher molecular anisotropy. For isotropic phases in Figure 5, the molecular length and width distributions of each LC compound expand. This broadness is much clearer in the molecular length distribution.

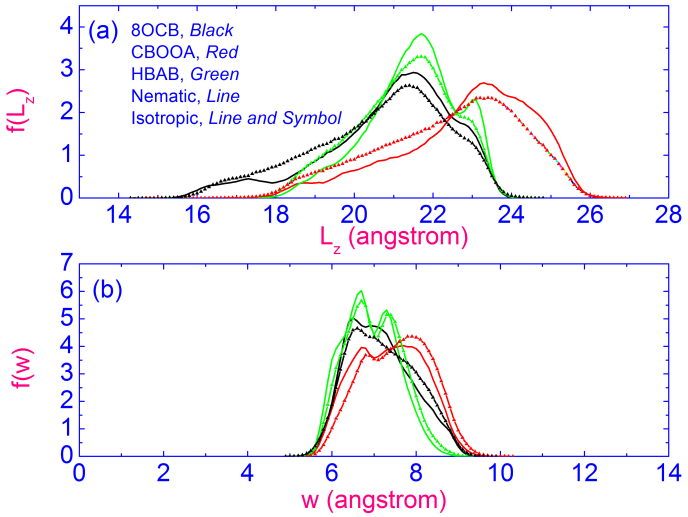

Figure 5. Distribution functions of molecular (a) length and (b) width for 8OCB, CBOOA, and HBAB.

Table 2 collects the results of principal inertia tensor components, biaxiality $\langle \lambda_I \rangle$, and anisotropy, $\langle \Delta I \rangle$, of the inertia tensor. The average values in Table 2, $I_{xx} \cong I_{yy} > I_{zz}$, reveal that the molecules are in prolate form on average, with negligible biaxialities, which are considerably lower than the molecular dimension biaxialities. The biaxiality obtained from the molecular dimension for 8OCB in this study is higher than those for Schiff bases and the one computed for 8CB [46]. The values of the inertia tensor anisotropy $\langle \Delta I \rangle$, of the molecules with imine groups are greater than this value of 8OCB. The greatest inertia tensor anisotropy belongs to HBAB with a short alkyl chain. The result obtained from the inertia tensor anisotropy is similar to the result obtained from the shape anisotropy. The inertial tensor anisotropy distribution peaks of Schiff bases are sharper than that of 8OCB (Figure 6) because of the presence of a flexible imine spacer between the rigid aromatic rings. The tensor anisotropy peak of HBAB, which has a short alkoxy chain, is the highest. For isotropic phases in Figure 6, the curves in the distributions are broader, as in the other distributions in the isotropic phase.

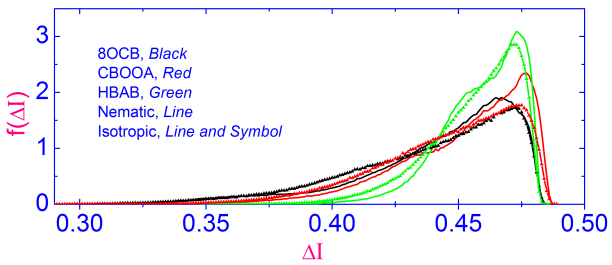

Figure 6. Distribution functions of the inertial tensor anisotropy for 8OCB, CBOOA, and HBAB.

4. Discussion

By using MD simulations, some structural properties of 8OCB, CBOOA, and HBAB compounds in the nematic and isotropic phases were calculated. The distributions of the angles between some defined vectors imply that the two phenyl rings are along the molecular axis in 8OCB, whereas the imine (-CH=N-) linking group of two Schiff bases induces a stepped core structure while the linearity is maintained. Furthermore, the imine increases the molecular length, width, aspect ratio, and shape anisotropy and decreases the biaxiality because it causes extra flexibility. The aspect ratio of the Schiff bases was found to be almost the same. However, the molecular dimensions and the biaxiality of HBAB are smaller than those of CBOOA and its shape anisotropy is greater. That HBAB has a shorter alkyl chain when it is compared to CBOOA may cause this result, if the difference in the positions of nitrogen atoms in the imine groups of the CBOOA and HBAB molecules is disregarded. The peak positions of the distribution for HBAB in Figure 4a show that its rigid part is almost along the molecular axis and this result explains the greater molecular anisotropy of HBAB. All distributions of HBAB except the one in Figure 3a are narrower than those of CBOOA. The diagonal elements of the inertia tensor show that 8OCB, CBOOA, and HBAB are in prolate form on average and the computed negligible biaxiality values show that these molecules are uniaxial. The computed molecular dimensions and anisotropies for all mesogens in the isotropic phase are smaller than those in the nematic phase and all distributions in the isotropic phase widen because the flexibility of the molecules increases with temperature and especially the contribution of bent conformations of alkyloxy chain increases, and so molecular biaxiality increases.

From the present results it appears that the MD simulation method is able to reproduce some structural properties of 8OCB, CBOOA, and HBAB compounds in the nematic and isotropic phases.

Acknowledgments

The computations were performed at the ULAKBİM High Performance Computing Center, which is gratefully acknowledged. This study was partially supported by Ege University under the BAP 2011 Fen 043 and 2011 Fen 044 projects. The author is deeply grateful for the financial support of Ege University.

References

[1] Lee, J. H.; Liu, D. N.; Wu, S. T. *Introduction to Flat Panel Displays*, 1st ed.; John Wiley & Sons: Chichester, UK, 2008.

[2] Smith, C. A. *Circuit World* **2008**, *34*, 35-41.

[3] Kelly, S. M. *Flat Panel Displays: Advanced Organic Materials*; The Royal Society of Chemistry: Cambridge, UK, 2000.

[4] Bouligand, Y. *Comptes Rendus Chimie* **2008**, *11*, 281-296.

[5] Chandrasekhar, S. *Liquid Crystals*, 2nd ed.; Cambridge University Press: Cambridge, UK, 1992.

[6] De Gennes, P. G.; Prost, J. *The Physics of Liquid Crystals*, 2nd ed.; Clarendon Press: Oxford, UK, 1993.

[7] Luckhurst, G. R.; Veracini, C. A. *The Molecular Dynamics of Liquid Crystals*; Kluwer Academic Press: London, UK, 1994.

[8] Singh, S; Dunmur, D. A. *Liquid Crystals Fundamentals*; World Scientific Press: Singapore, 2002.

[9] Satoh, K. *J. Chem. Phys.* **2006**, *125*, 204902.

[10] Toriumi, H.; Yoshida, M.; Kamiya, N.; Takeuchi, M. *Mol. Cryst. Liq. Cryst.* **2003**, *402*, 31-42.

[11] Phuong, N. H.; Germano, G.; Schmid, F. *J. Chem. Phys.* **2001**, *115*, 7227-7234.

[12] Zakharov, A. V.; Maliniak, A. *Eur. Phys. J. E* **2001**, *4*, 85-91.

[13] Peláez, J.; Wilson, M. *Phys. Chem. Chem. Phys.* **2007**, *9*, 2968-2975.

[14] Cheung, D. L.; Clark, S. J.; Wilson, M. R. *J. Chem. Phys.* **2004**, *121*, 9131-9139.

[15] Zakharov, A. V.; Dong, R. Y. *Eur. Phys. J. E* **2001**, *6*, 3-6.

[16] Kuwajima, S.; Manabe, A. *Chem. Phys. Lett.* **2000**, *332*, 105-109.

[17] Zakharov, A. V.; Komolkin, A. V.; Maliniak, A. *Phys. Rev. E* **1999**, *59*, 6802-6807.

[18] Bennett, L.; Hess, S. *Phys. Rev. E* **1999**, *60*, 5561-5567.

[19] Zakharov, A. V.; Dong, R. Y. *Phys. Rev. E* **2001**, *64*, 031701.

[20] Zakharov, A. V.; Mirantsev, L. V. *Phys. Solid State* **2003**, *45*, 183-188.

[21] Berardi, R.; Muccioli, L.; Zannoni, C. *ChemPhysChem* **2004**, *5*, 104-111.

[22] Tiberio, G.; Muccioli, L.; Berardi, R.; Zannoni, C. *ChemPhysChem* **2009**, *10*, 125-136.

[23] Cacelli, I.; Prampolini, G.; Tani, A. *J. Phys. Chem. B* **2005**, *109*, 3531-3538.

[24] Cacelli, I.; Gaetani, L. D.; Prampolini, G.; Tani, A. *J. Phys. Chem. B* **2007**, *111*, 2130-2137.

[25] Gray, G. W.; Harrison, K. J. *Symp. Faraday Soc.* **1971**, *5*, 54-67.

[26] Schadt, M.; Helfrich, W. *Appl. Phys. Lett.* **1971**, *18*, 127-128.

[27] Schadt, M.; Müller, F. *Rev. Phys. Appl.* **1979**, *14*, 265-274.

[28] Gray, G. W.; Kelly, S. M. *J. Mater. Chem.* **1999**, *9*, 2037-2050.

[29] Cladis, P. E. *Phys. Rev. Lett.* **1975**, *35*, 48-51.

[30] Cladis, P. E.; Bogardus, R. K.; Daniels, W. B.; Taylor, G. N. *Phys. Rev. Lett.* **1977**, *39*, 720-723.

[31] Kleinhans, H. D.; Schneider, G. M.; Shashidhar, R. *Mol. Cryst. Liq. Cryst.* **1983**, *103*, 255-259.

[32] Hess, B.; Kutzner, C.; van der Spoel, D.; Lindahl, E. *J. Chem. Theory Comp.* **2008**, *4*, 435-447.

[33] Jorgensen, W. L.; Tirado-Rives, J. *P. Natl. Acad. Sci. USA* **2005**, *102*, 6665-6670.

[34] Jorgensen, W. L.; Tirado-Rives, J. *J. Am. Chem. Soc.* **1988**, *110*, 1657-1666.

[35] Hauptmann, S.; Mosell, T.; Reiling, S.; Brickmann, J. *Chem. Phys.* **1996**, *208*, 57-71.

[36] Breneman, C. M.; Wiberg, K. B. *J. Comp. Chem.* **1990**, *11*, 361-373.

[37] Frisch, M. J.; Trucks, G. W.; Schlegel, H. B.; Scuseria, G. E.; Robb, M. A.; Cheeseman, J. R.; Montgomery, J. A.; Vreven, T. Jr; Kudin, K. N.; Burant, J. C. et al. *GAUSSIAN03 (Revision B.04)*; Gaussian, Inc.: Pittsburgh, PA, USA, 2003.

[38] Darden, T.; York, D.; Pedersen, L. *J. Chem. Phys.* **1993**, *98*, 10089-10092.

[39] Bussi, G.; Donadio, D.; Parrinello, M. *J. Chem. Phys.* **2007**, *126*, 014101.

[40] Berendsen, H. J. C.; Postma, J. P. M; DiNola, A.; Haak, J. R. *J. Chem. Phys.* **1984**, *81*, 3684-3690.

[41] Sen, M. S.; Brahma, P.; Roy, S. K.; Mukherjee, D. K.; Roy, S. B. *Mol. Cryst. Liq. Cryst.* **1983**, *100*, 327-340.

[42] Wittebort, R. J.; Subramanian, R.; Kulshreshtha, N. P.; DuPré, D. B. *J. Chem. Phys.* **1985**, *83*, 2457-2466.

[43] Miyajima, N.; Nakamura, N.; Chihara, H. *Mol. Cryst. Liq. Cryst.* **1982**, *89*, 151-169.

[44] Cladis, P. E. *Liq. Cryst.* **1998**, *24*, 15-19.

[45] Madsen, L. A.; Dingemans, T. J.; Nakat, M.; Samulski, E. T. *Phys. Rev. Lett.* **2004**, *92*, 145505.

[46] Capar, M. I.; Cebe, E. *J. Comput. Chem.* **2007**, *28*, 2140-2146.